

Mesh convergence error estimations for compressible inviscid fluid flow over airfoil cascades using multiblock structured mesh

A. Tater^{a,*}, J. Holman^a

^a*Department of Technical Mathematics, Faculty of Mechanical Engineering, Czech Technical University in Prague, Karlovo náměstí 13, Prague, Czech Republic*

Received 27 March 2023; accepted 21 June 2023

Abstract

This work deals with estimations of errors, which are a consequence of a finite spatial discretisation that appears while solving differential equation numerically. More precisely, it deals with the estimation of errors that occur while computing compressible inviscid fluid flow over 2D airfoil cascades. This flow is described by the 2D Euler equations that are solved by the finite volume method in their conservative form. Numerical computations are performed on structured meshes consisting of four blocks, so the number of cells in the mesh can be easily adjusted. In this work, two estimation methods are used. Firstly, the grid convergence index is used to estimate the amount of cells needed to obtain certain accuracy of the solution. Secondly, the Richardson extrapolation is used to approximate the exact solution from a series of solutions obtained with meshes of different sizes. This analysis is performed on a well-known compressor cascade, which is composed of NACA 65 series airfoils. The obtained results should lead to a reasonable choice of the number of elements in a computational mesh based on the required accuracy of the solution and therefore also to computational time reduction while performing airfoil cascade computations. The results indicate that even for very precision demanding applications, 100 000 is a sufficient number of cells in a mesh.

© 2023 University of West Bohemia.

Keywords: airfoil cascade, grid convergence index, 2D inviscid fluid flow, NACA 65 series, structured mesh

1. Introduction

Nowadays, when computational fluid mechanics has prevailed in the scientific and commercial community as a tool for performance prediction and the design of various technical devices, it is the right time to carefully study errors that occur while solving systems of partial differential equations related to fluid mechanics numerically. With the rapid increase in computing power over the past decades, it is currently quite common to simulate complicated 3D turbulent flows on computational meshes with the number of tens to hundreds of millions cells. This widespread of technology, which became available to almost everyone, results in frequent neglect of essential standard practices such as establishing the independence of the solution on the computational mesh. This very important practice is described and applied in this work.

This paper deals with the research of discretisation errors that appear while solving 2D inviscid flow of compressible fluid through a compressor airfoil cascade using the finite volume method. This flow problem could be presently considered obsolete, when many methods of turbulence modelling are available, but there are several problems where this simplified view of reality would be sufficient. Primarily, the cascades represent cylindrical sections with 3D blades and their subsequent development into a plane. With this procedure, the flow through individual

*Corresponding author. Tel.: +420 602 940 806, e-mail: adam.tater@fs.cvut.cz.
<https://doi.org/10.24132/acm.2023.827>

cascades can be simulated and the shape of the airfoils can be designed and optimised. Finally, the resulting 3D blade can be assembled and interpolated from individual cascades. In compressors, the effect of compressibility is generally more dominant than the viscous effects. This supports the idea that, for example, the pressure distribution along the airfoil can be predicted with good accuracy even by inviscid flow simulations. So when it comes to optimisation of pressure distribution along the airfoil, it seems to be appropriate to use the system of equations describing inviscid fluid flow. This system has several advantages for optimisation tasks, like less consumption of computational power and fewer stability issues. However, this all depends on whether the flow solutions are sufficiently accurate.

In this work, emphasis is placed on mesh convergence, which is a topic directly related to the number of cells in a computational mesh. This further has a major effect on the computational time. Many papers examine the grid convergence in turbomachinery tasks. In [28], Shin and Ragab simulated 3D incompressible flow with the Spalart-Allmaras turbulence model through a highly staggered compressor cascade with a tip clearance on three different meshes. In [1], Akçayöz studied performance increase and noise reduction in axial compressor cascades with plasma actuation. The grid convergence study was performed for each cascade with three meshes, both structured and unstructured. In [27], Schneider and Kožulović researched flow characteristics of axial compressor tandem cascades at large off-design incidence angles and performed a mesh convergence study on structured meshes. In [7], Busse et al. numerically investigated effects of the steady wake and the tip clearance vortex interaction in a compressor cascade, where a mesh convergence study was performed on multiblock structured mesh. In [21], Li et al. defined effective end wall profiling rules for highly loaded compressor cascades and performed mesh convergence study on three meshes. In [20], Li et al. used a blended blade and established an end wall method in compressor cascades, six meshes were used in the mesh convergence study. Giorgi et al. [9] compared different plasma actuation strategies for aeroelastic control on a linear compressor cascade and supported their results by a mesh convergence study. In [35], Yin and Durbin performed a detached eddy simulation of transition in a linear compressor cascade and used several meshes to ensure mesh independence. Kiss et al. [19] investigated transonic turbine cascade flow and studied mesh convergence on a C-shaped mesh. In [14], Hildebrandt and Fottner performed a numerical study of the influence of mesh refinement and turbulence modelling on the flow field inside a highly loaded turbine cascade. In [23], Kumar and Govardhan studied the topology of flow in a turbine cascade and validated results on three meshes.

There are also many applications other than in turbomachinery that use mesh convergence for result validation. Warren et al. [33] dealt with mesh convergence of adaptive methods applied in supersonic flow around NACA 0012 airfoil. A mesh convergence study on this airfoil was also performed by Vassberg and Jameson [30] and Diskin et al. [11]. In [4], Blain et al. investigated the influence of mesh convergence on the prediction of hurricane storm surge. De Sterck et al. [10] performed a characteristic analysis and mesh convergence study for magnetohydrodynamic flows with shocks. In [26], Salas presented several observations of mesh convergence. Longest and Vinchurkar [22] studied effects of mesh style and mesh convergence on particle deposition in bifurcating airway models. Ali et al. [2] published a mesh convergence study for direct numerical simulations of flow around a square cylinder at low Reynolds number. Hodis et al. [16] discussed mesh convergence errors in haemodynamic problems of patient-specific cerebral aneurysms. Oliveira et al. [24] performed a mesh convergence study of a cyclone separator using different mesh structures.

At the beginning of this paper, the system of partial differential equations describing 2D

inviscid compressible flow is mentioned. Next, the finite volume method is briefly presented and the used numerical flux is shown. It is also stated how to achieve the second order spatial accuracy and the time integration method. In the following sections, the problem of compressor cascades is formulated and the method of multiblock meshing is described. After that, the methodology of mesh convergence study is stated. The penultimate section presents the results of convergence study on the well-known NACA 65 series compressor cascade. Grid convergence index is calculated for various angles of attack and inflow velocities. The way how to use the Richardson extrapolation is shown and the number of cells needed for the precision of individual results are estimated. Finally, the results are discussed and conclusions are drawn.

2. Governing equations

Using the laws of mass, momentum and total energy conservation, the system of Euler equations can be derived by omitting viscous terms. The system can be found, for example, in [5, 15]. Since a 2D inviscid flow problem is considered in the present work, the 2D Euler equations can be written in vector form as follows

$$\frac{\partial \mathbf{W}}{\partial t} + \frac{\partial \mathbf{F}(\mathbf{W})}{\partial x} + \frac{\partial \mathbf{G}(\mathbf{W})}{\partial y} = \mathbf{0}, \quad (1)$$

where the individual vectors can be expressed as

$$\mathbf{W} = \begin{bmatrix} \rho \\ \rho u \\ \rho v \\ \rho E \end{bmatrix}, \quad \mathbf{F}(\mathbf{W}) = \begin{bmatrix} \rho u \\ \rho u^2 + p \\ \rho uv \\ (\rho E + p)u \end{bmatrix}, \quad \mathbf{G}(\mathbf{W}) = \begin{bmatrix} \rho v \\ \rho vu \\ \rho v^2 + p \\ (\rho E + p)v \end{bmatrix}, \quad (2)$$

where u and v are the components of the velocity vector. The variables ρ , p , and E denote the density, static pressure and total energy, respectively. As the previously mentioned system (1) has more variables than equations, it is necessary to close it using some constitutive relation. For this work, the perfect gas equation, firstly published by Clausius in [8], was chosen. It can be written as

$$\frac{p}{\rho} = R_{spec} T, \quad (3)$$

where R_{spec} and T are the specific gas constant and the thermodynamic temperature, respectively. It can be further modified with the Mayer's relation into the following form:

$$p = (\kappa - 1) \left[\rho E - \frac{1}{2} \rho (u^2 + v^2) \right], \quad (4)$$

which is the form used in the following.

3. Methods

The finite volume method is used in this paper. This method is obtained by integrating the previous system of equations (1) over a general finite volume. Next, after the application of the Green's theorem and a few adjustments, it is possible to write the result as

$$\frac{d\mathbf{W}_{ij}}{dt} = - \frac{1}{\|\Omega_{ij}\|} \oint_{\partial\Omega_{ij}} (\mathbf{F}n_x + \mathbf{G}n_y) ds, \quad (5)$$

where the argument of the integral can be rewritten using the transformation matrix \mathbf{T} as

$$\mathbf{F}n_x + \mathbf{G}n_y = \mathbf{T}^{-1}\mathbf{F}(\mathbf{T}\mathbf{W}) = \tilde{\mathcal{F}}, \quad \mathbf{T} = \begin{bmatrix} 1 & 0 & 0 & 0 \\ 0 & n_x & n_y & 0 \\ 0 & -n_y & n_x & 0 \\ 0 & 0 & 0 & 1 \end{bmatrix}. \quad (6)$$

After substituting (6) into (5), admitting the fact that the volumes are quadrilaterals and by replacing the physical flux \mathcal{F} with the numerical flux $\tilde{\mathcal{F}}$, equation (5) can be rewritten as

$$\frac{d\mathbf{W}_{ij}}{dt} = -\frac{1}{\|\Omega_{ij}\|} \sum_{k=1}^4 \tilde{\mathcal{F}}_k(\mathbf{W}_{ij}) \|S_k\|. \quad (7)$$

The approximate rotated-hybrid Riemann solver published by Holman and Fürst [17] was chosen for its favourable properties when solving inviscid physical fluxes. It is a combination of the well-known HLLC numerical flux stated by Toro et al. [29] and the HLL numerical flux published by Harten et al. [13]. This combination ensures accuracy because of the HLLC flux and its three wave structure and also the absence of the carbuncle phenomenon due to the more dissipative HLL flux.

In order to achieve a second order accuracy, gradients of variables were estimated by the spatial least squares method using the neighbouring cells. These gradients were then used to extrapolate values of variables from cell centres to wall centres. However, a solution defined in this way would show non-physical oscillations, reconstructed quantities could go beyond all limits and such a calculation would lead to misleading results. Therefore, it is necessary to limit the values of gradients in some reasonable way which may be achieved by introducing a limiter function. In this paper, the Venkatakrishnan’s limiter published in [31] was used. This is an improvement of the Barth–Jespersen’s limiter [3]. Since this work seeks stationary solutions using a time-dependent simulation, it is important to employ a time integration method. For this purpose, the three-step Runge-Kutta method of second order accuracy was chosen [32].

4. Problem formulation and mesh topology

An axial compressor is a highly complex and sophisticated piece of turbomachinery, so it is quite common to decompose simulations of flow through this machine into several subtasks, which can be further simplified [12]. These simplifications are often used for design and verification.

Fig. 1 schematically shows the conversion of a 3D compressor rotor problem in cylindrical coordinates into a 2D airfoil cascade in the Cartesian coordinate system. Furthermore, the inlet Γ_I , the outlet Γ_O and the periodic boundary conditions are shown on the right side of Fig. 1. The conversion also means that a naturally transient problem is transformed into a stationary problem, where the angle of attack and the velocity of incoming flow is set to match the conditions in the compressor.

The axial compressor cascade, which is the subject of research in this work, is composed of NACA 65-(12)10 airfoils. The geometry of this airfoil is described in [6]. The geometrical specifications and numerical simulations performed on this cascade were published by Hwang and Liu in [18]. The boundary conditions (BC) for the mesh convergence study are listed in Table 1. It also follows that the study is carried out by the change of the incidence angle and the outlet pressure.

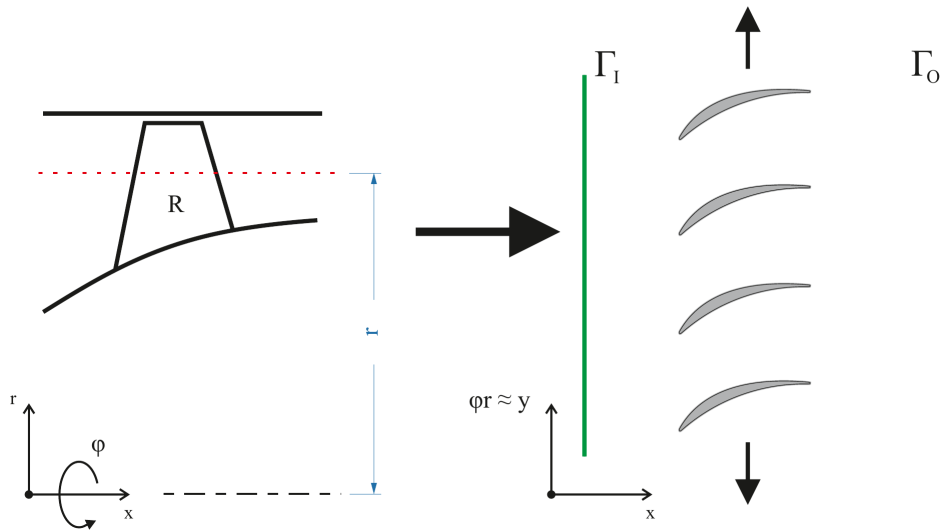


Fig. 1. Transformation of a 3D rotor stage into a 2D cascade

Table 1. Airfoil cascade boundary conditions

BC	Variable	Value	Unit
Γ_I	total pressure p_0^I	101 325	Pa
	total temperature T_0^I	300	K
	incidence angle α^I	43 ÷ 47	°
Γ_O	pressure p^O	88 500 ÷ 96 000	Pa

The topological structure of the computational mesh can be seen in Fig. 2a. The computational domain Ω is divided into four blocks. It starts with the aerodynamic profile around which a hyperbolic O-shaped mesh Ω_1 is generated. The block Ω_3 is an elliptical mesh formed from Ω_1 in the opposite direction of the flow. Its right border is given by the block Ω_1 and its left side is the inlet boundary Γ_I at a distance of one chord length from the aerodynamic profile. The upper and lower limits are defined so that excessively skewed cells were not formed. The same goes for the block Ω_4 , which points in the direction of the flowing fluid from the trailing edge of the profile. The left edge is formed by the block Ω_1 and the right one is formed as the outlet boundary Γ_O at a distance of two chords from the profile. The upper and lower sides are defined similarly as in the case of block Ω_3 . The last block Ω_2 has left and right borders defined in the same way as the previous two blocks. The upper limit of the block is defined as the unification of the lower sides of blocks Ω_1 , Ω_3 , and Ω_4 . In order to observe the periodicity, it is necessary that the lower surface of this block is formed by a union of upper sides of blocks Ω_1 , Ω_3 , and Ω_4 shifted in the y -direction by the distance of two neighbouring airfoils. As in the previous two cases, this block is also generated elliptically. The computational domain Ω is thus formed as a four-block mesh.

The boundary conditions are also shown in Fig. 2a. The linear periodicity Γ_P is coloured in red and the inviscid wall BC Γ_W is gray. The blocks are connected by the connectivity BC Γ_C which is coloured in black. The inlet and outlet BCs are green and blue, respectively. A generated multiblock mesh around the airfoil is shown in Fig. 2b.

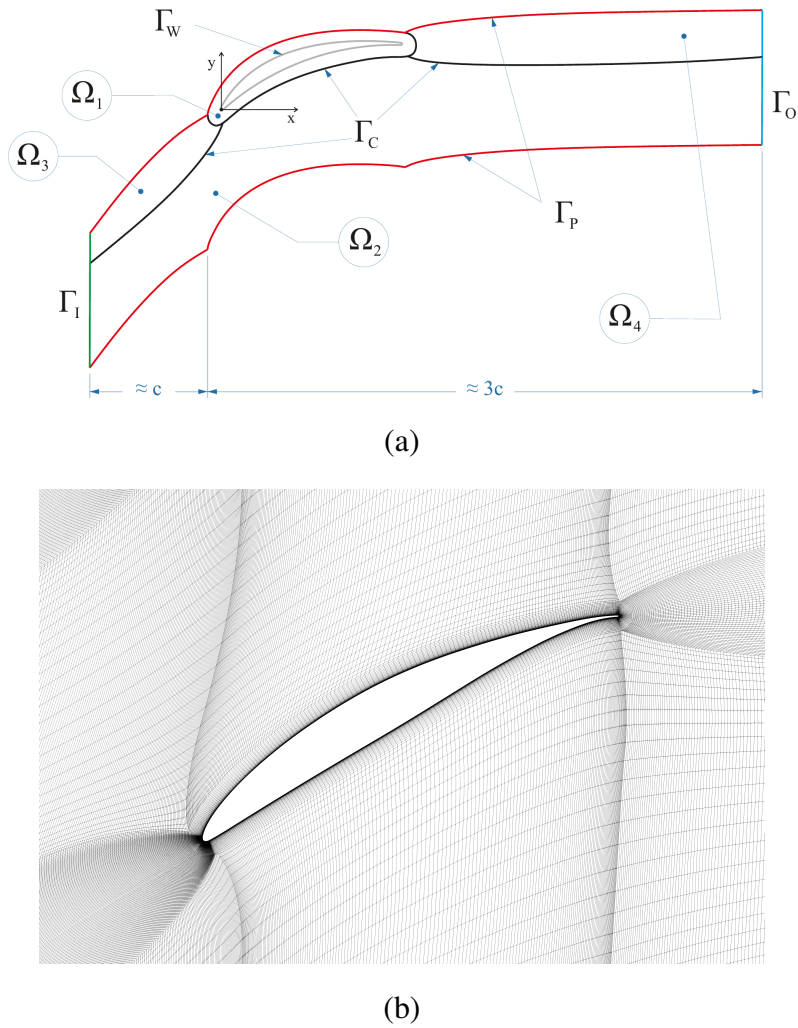


Fig. 2. Mesh topology description: (a) mesh block division and boundaries, (b) visualisation of the finest mesh generated for the mesh convergence analysis

5. Mesh convergence study

The mesh convergence study is a straightforward method for determining the discretisation error in a numerical simulation. The method involves performing the simulation on successively finer meshes. As the mesh is refined, the spatial discretisation errors should asymptotically approach zero, when excluding computer rounding errors.

Some scalar quantity must be specified for the purpose of this study. In this case, minimal static pressure on the airfoil \mathcal{P} was chosen. Three successively finer meshes were generated with the refinement ratio $r = 2$, which means that the finer mesh has twice as many cells as the coarser mesh in both spatial directions. All three meshes are listed in Table 2 together with the number of cells.

Since the parameter r is a constant, the order of convergence \mathcal{O} can be obtained directly from three solutions as follows [25]

$$\mathcal{O} = \frac{\ln\left(\frac{\mathcal{P}_1 - \mathcal{P}_2}{\mathcal{P}_2 - \mathcal{P}_3}\right)}{\ln(r)}. \quad (8)$$

After the evaluation of the convergence order, the Richardson extrapolation, described by Zlatev

Table 2. Meshes generated and used in the convergence study

Mesh	Coarse '1'	Medium '2'	Fine '3'
Normalised mesh spacing	4	2	1
Number of cells	4 382	17 528	70 112

et al. [36], can be applied to the two finest meshes. It uses them to obtain an estimate of the value of 'exact' solution at zero mesh spacing as

$$\mathcal{P}_{ext} = \mathcal{P}_3 + \frac{\mathcal{P}_3 - \mathcal{P}_2}{r^{\mathcal{O}} - 1}. \quad (9)$$

According to Roache [25], the grid convergence index (GCI) is a preferred way to estimate discretisation errors. It is a measure of percentage the computed value is away from the value of the asymptotic numerical value. It indicates an error band on how far the solution is from the asymptotic value and how much the solution would change with additional grid refinement. A small value of GCI indicates that the computation is within the asymptotic range. It can be computed as follows

$$\text{GCI} = \frac{F_S |\varepsilon|}{r^{\mathcal{O}} - 1} \cdot 100, \quad \varepsilon = \frac{\mathcal{P}_{finer} - \mathcal{P}_{coarser}}{\mathcal{P}_{finer}}. \quad (10)$$

In [34], the safety factor F_S is recommended by Wilcox to be $F_S = 1.25$ when three or more meshes are used. Two grid convergence indexes GCI_{12} and GCI_{23} can be obtained from three meshes. Another important quantity can be estimated by using the grid convergence index. The specific grid refinement factor r^* can be estimated from the highest allowable error GCI^* as

$$r^* = \left(\frac{\text{GCI}^*}{\text{GCI}_{12}} \right)^{\frac{1}{\mathcal{O}}}. \quad (11)$$

This enables to estimate a sufficient number of mesh cells for specific precision of the simulation.

6. Results

A computational study of mesh convergence was performed by changing the incidence angles and outlet pressures. The incidence angles were chosen as the cascade's design incidence 45° , two negative incidence angles (44° , 43°), and two positive incidence angles (46° , 47°). Four outlet pressures were chosen to explore the subsonic and lower transonic velocity regimes. This should cover the standard working conditions of the studied cascade. The airfoil minimal pressure \mathcal{P} was observed in each of these 20 simulations for all three meshes. The results are presented in Table 3.

Using the data from Table 3, the order of convergence \mathcal{O} was estimated using (8) for each combination of the incidence angle and the outlet pressure. The results are listed in the upper section of Table 3. The order of convergence computed for each simulation is further displayed as a 3D graph shown in Fig. 3. From the data and the graphical representation, it can be noted that the values of order of convergence oscillate around the number 2. This is the expected result, because second order schemes are used. Furthermore, there can be also seen

Table 3. Results of the minimal airfoil pressure \mathcal{P} depending on the incidence angle α^I [$^\circ$], outlet pressure p^O [Pa] and mesh; results of the convergence order \mathcal{O} and the grid convergence indexes (GCI_{12} , GCI_{23}) depending on the incidence angle and the outlet pressure

		\mathcal{P}_1					\mathcal{O}				
p^O	α^I	43	44	45	46	47	43	44	45	46	47
88 500		57 943	54 662	50 893	47 076	43 236	2.57	1.57	1.47	2.20	2.80
91 000		68 554	66 502	64 113	61 475	58 575	2.38	2.33	1.39	1.39	1.58
93 500		77 629	76 230	74 726	73 052	70 991	2.28	1.99	1.33	2.00	2.13
96 000		85 756	84 902	84 003	82 935	81 043	2.21	1.52	1.89	2.32	2.10
		\mathcal{P}_2					GCI_{12}				
88 500		56 130	51 704	46 139	40 583	36 146	0.82	3.63	7.27	5.56	4.11
91 000		68 021	65 761	63 123	59 482	54 915	0.23	0.35	1.21	2.57	4.18
93 500		77 360	75 921	74 077	71 702	68 870	0.11	0.17	0.72	0.78	1.14
96 000		85 606	84 730	83 500	82 024	79 212	0.06	0.14	0.28	0.35	0.88
		\mathcal{P}_3					GCI_{23}				
88 500		55 825	50 708	44 424	39 171	35 129	0.14	1.25	2.72	1.25	0.61
91 000		67 918	65 614	62 745	58 723	53 693	0.04	0.07	0.47	0.99	1.43
93 500		77 304	75 844	73 820	71 366	68 384	0.02	0.04	0.29	0.19	0.26
96 000		85 573	84 670	83 364	81 841	78 786	0.01	0.05	0.08	0.07	0.21

an interesting decline in the order of convergence while performing simulations with the design incidence angle. Another interesting finding is the fact that the values of the convergence order differ more while performing simulations with lower outlet pressures. This can be explained by analysing the flow fields, where simulations with the incidence angle of (46° , 47°) in the case of $p^O = 91\,000$ Pa and computations with the incidence angle of (44° , 45°) in the case of $p^O = 88\,500$ Pa are very close to or are forming small supersonic regions. Then, the mesh can easily change the characteristics of the flow, resulting in higher errors. On the other hand, in the

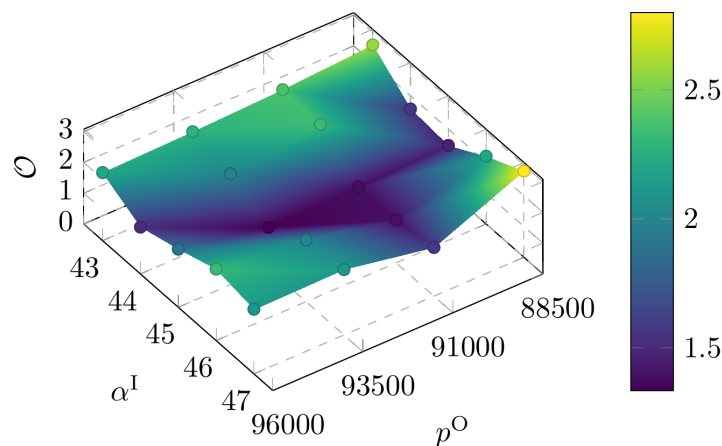


Fig. 3. 3D graph of the convergence order depending on the incidence angle and the outlet pressure

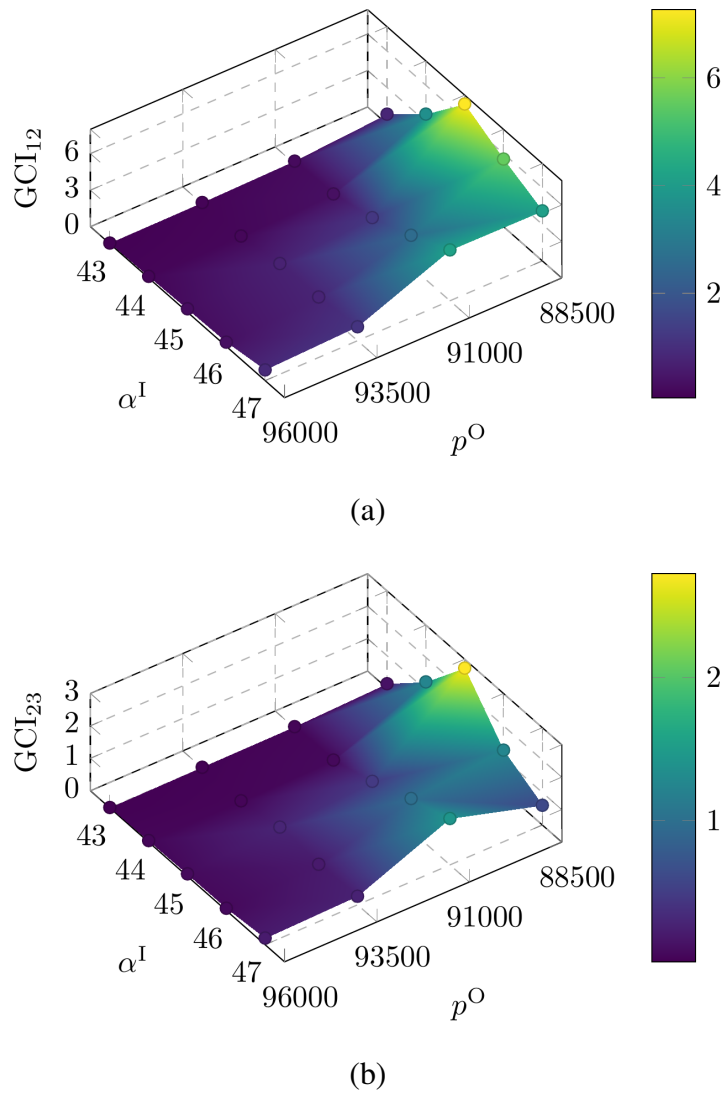


Fig. 4. 3D representation of grid convergence indexes: (a) GCI_{12} , (b) GCI_{23}

case of $\alpha^I = 47^\circ$ and $p^O = 88\,500$ Pa, there is a fully developed supersonic region ending with a shock wave and the order of convergence is the highest.

Using the data from Table 3, the order of convergence \mathcal{O} from Table 4 and the formula (10), the grid convergence indexes were computed between meshes 1–2 and 2–3 for each combination of the incidence angle and the outlet pressure. The results of these calculations are given in the middle and lower parts of Table 3. These data are also displayed in Fig. 4. From the graphical representation of the data, it is clear that possible discretisation errors increase when the flow transitions to a transonic regime. Furthermore, in both quantities GCI_{12} and GCI_{23} , the errors

Table 4. Estimations of the number of cells needed to achieve a specific accuracy

GCI^*	1	0.1	0.01	0.001
\bar{r}^*	1.415 2	0.444 0	0.146 2	0.049 9
Est. number of cells	8 751	88 912	820 122	7 037 854

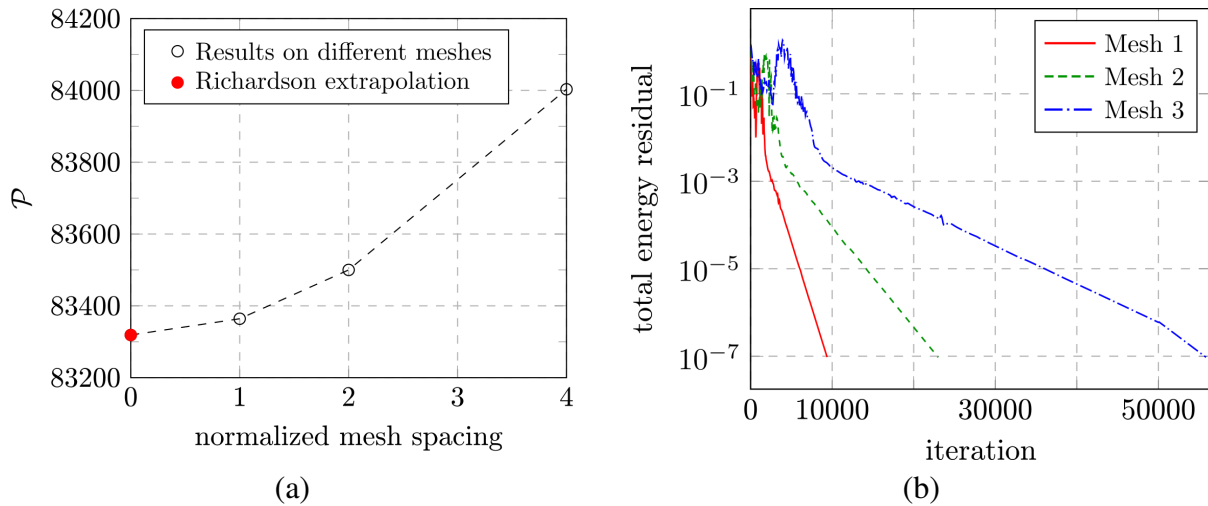


Fig. 5. Example of the Richardson extrapolation used on simulations with the design incidence angle and the highest outlet pressure: (a) graphic representation of the extrapolation, (b) plot of individual total energy residuals for each mesh

are very low in the case of the negative incidence angle $\alpha^I = 43^\circ$ and the two highest outlet pressures.

An example of the Richardson extrapolation (9) applied to the data obtained from the simulations with the design incidence angle and the highest outlet pressure is shown in Fig. 5a. The solution obtained by the extrapolation is marked by a red dot and is theoretically of the fourth order of accuracy. Individual total energy residuals associated with the usage of different meshes in the previously mentioned simulation setup are plotted in Fig. 5b.

Additional view of the errors in the flow fields can be provided by Figs. 6 and 7. On the left side of those figures, pressure fields are shown for the design incidence angle and outlet pressures of (96 000, 88 500) Pa, respectively. On the right side of those figures, the field of absolute values of pressure differences between the results obtained on mesh 2 and 3 is displayed. In Fig. 6b, the main errors are located near the flow stagnation point, where the pressure gradient is high, and between the suction and pressure sides of the airfoils. In the case of Fig. 7b, the errors are to the greatest extent located in the forming supersonic region and mainly in the place where the shock wave is formed.

At last but not least, equation (11) was used to estimate the specific refinement ratio to achieve specific discretisation errors of 1, 0.1, 0.01, and 0.001 percent. It was computed with the mean value of GCI_{12} from all performed simulations, by substituting it into (11). The obtained specific refinement ratios and estimated numbers of cells can be seen in Table 4. From these data, it follows that the number of cells needed for an order of magnitude improvement in discretisation errors grows rapidly.

7. Conclusions

In this paper, a method for the estimation of discretisation errors during inviscid fluid flow through compressor cascades was presented. Firstly, governing equations of the inviscid flow were stated. Secondly, methods used in this paper to solve those equations numerically were presented. After that, the compressor cascade problem was formulated and the meshing strategy was explained. As the last theoretical section, the mesh study methodology was presented and

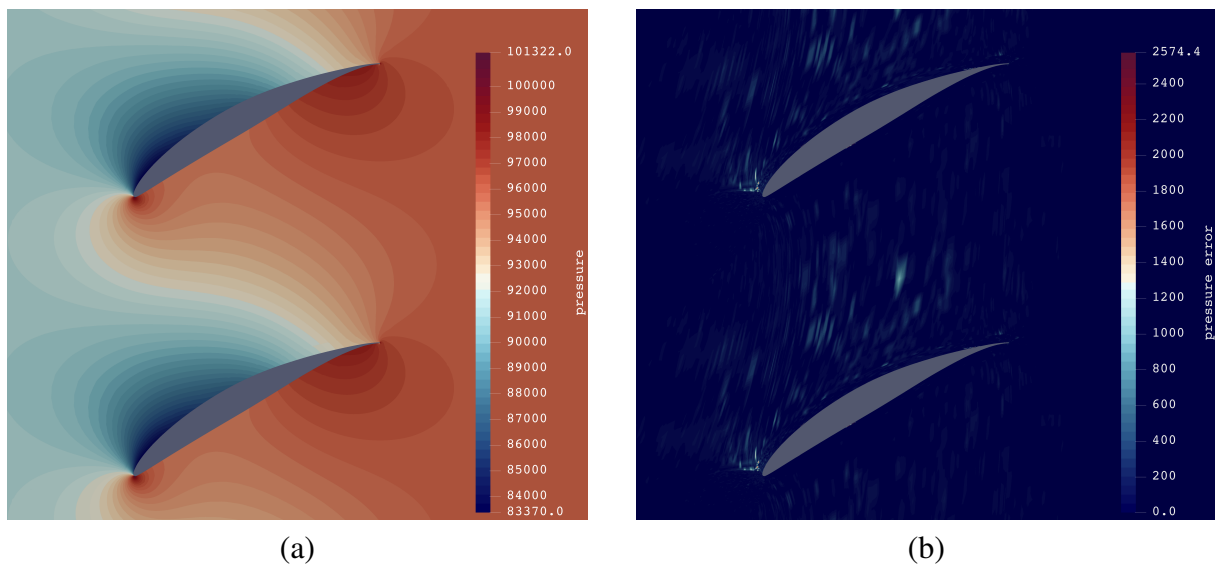


Fig. 6. Spatial visualisation of errors for the design incidence angle and the outlet pressure of 96 000 Pa: (a) pressure contours, (b) absolute value of pressure error

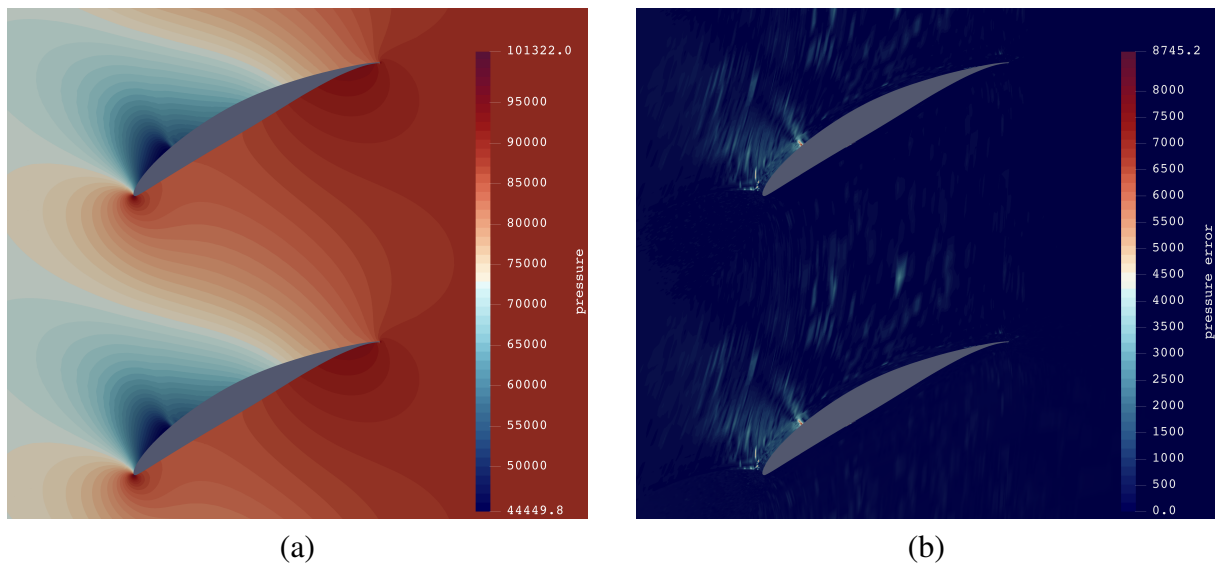


Fig. 7. Spatial visualisation of errors for the design incidence angle and the outlet pressure of 88 500 Pa: (a) pressure contours, (b) absolute value of pressure error

meshes further used were defined. Finally, the results of the mesh convergence study were presented both in tables and figures.

Several conclusions and recommendations can be drawn from the obtained results. The order of convergence is the highest for negative incidence angles and in the case of a fully developed local supersonic region. Interesting features are the low values of the convergence order for the design incidence angle. When it comes to GCI percentage errors, the results speak much clearer. Again, there is a clear trend that the design angle errors are higher than the negative and positive incidence angles. However, the more important finding is that in both GCI_{12} and GCI_{23} cases, the percentage errors increase with decreasing outlet pressures. Furthermore, an example of the Richardson extrapolation and a comparison of individual residual plots using different computational meshes was shown. This shows the computational complexity of simulations

on meshes with a larger number of cells. From the graphical analysis of the errors in the flow field, it can be concluded that refining the computational mesh makes a lot of sense only in the space between the airfoils and, more precisely, only in the vicinity of the suction side. Finally, the number of cells needed to achieve a certain accuracy of the calculations was investigated. Based on the results, it should be possible to determine a reasonable number of cells for this task. It seems that around 100 000 cells should be enough even for high precision demanding applications.

Acknowledgements

This work was supported by the grant agency of the Czech Technical University in Prague, grant No. SGS22/148/OHK2/3T/12 and from the ESIF, EU Operational Programme Research, Development and Education, and from the Center of Advanced Aerospace Technology (CZ.02.1.01/0.0/0.0/16019/0000826), Faculty of Mechanical Engineering, Czech Technical University in Prague.

References

- [1] Akçayöz, E., Performance increase and noise reduction in axial compressor cascades with plasma actuation, Ph.D. thesis, École Polytechnique de Montréal, Montréal, 2012.
- [2] Ali, M. S. M., Doolan, C. J., Wheatley, V., Grid convergence study for a two-dimensional simulation of flow around a square cylinder at a low Reynolds number, Proceedings of the 7th International Conference on CFD in the Minerals and Process Industries, Melbourne, 2009, pp. 1–6.
- [3] Barth, T., Jespersen, D., The design and application of upwind schemes on unstructured meshes, Proceedings from the 27th Aerospace Sciences Meeting, Reno, 1989, pp. 1–12.
<https://doi.org/10.2514/6.1989-366>
- [4] Blain, C. A., Westerink, J. J., Luettich Jr, R. A., Grid convergence studies for the prediction of hurricane storm surge, International Journal for Numerical Methods in Fluids 26 (4) (1998) 369–401.
[https://doi.org/10.1002/\(SICI\)1097-0363\(19980228\)26:4%3C369::AID-FLD624%3E3.0.CO;2-0](https://doi.org/10.1002/(SICI)1097-0363(19980228)26:4%3C369::AID-FLD624%3E3.0.CO;2-0)
- [5] Blazek, J., Computational fluid dynamics: Principles and applications, Butterworth-Heinemann, 2015. <https://doi.org/10.1016/C2013-0-19038-1>
- [6] Bogdonoff, S. M., Bogdonoff, H. E., Blade design data for axial-flow fans and compressors, Technical Report No. NACA-WR-L-635, Langley Aeronautical Laboratory, 1945.
- [7] Busse, P., Krug, A., Vogeler, K., Effects of the steady wake-tip clearance vortex interaction in a compressor cascade: Part II—Numerical investigations, Proceedings of ASME Turbo Expo 2014: Turbine Technical Conference and Exposition, Düsseldorf, 2014, pp. 1–13.
<https://doi.org/10.1115/GT2014-26121>
- [8] Clausius, R., The nature of the motion which we call heat, Annalen der Physik und Chemie 176 (3) (1857) 353–380. (in German) <https://doi.org/10.1002/andp.18571760302>
- [9] De Giorgi, M. G., Motta, V., Suma, A., Laforì, A., Comparison of different plasma actuation strategies for aeroelastic control on a linear compressor cascade, Aerospace Science and Technology 117 (2021) 1–14. <https://doi.org/10.1016/j.ast.2021.106902>
- [10] De Sterck, H., Csík, A., Abeele, D. V., Poedts, S., Deconinck, H., Stationary two-dimensional magnetohydrodynamic flows with shocks: Characteristic analysis and grid convergence study, Journal of Computational Physics 166 (1) (2001) 28–62. <https://doi.org/10.1006/jcph.2000.6640>
- [11] Diskin, B., Thomas, J. L., Rumsey, C. L., Schwöppe, A., Grid convergence for turbulent flows, Proceedings of the 53rd AIAA Aerospace Sciences Meeting, Kissimmee, 2015, pp. 1–50.
<https://doi.org/10.2514/6.2015-1746>
- [12] Farokhi, S., Aircraft propulsion, Chichester, John Wiley & Sons, 2014.

- [13] Harten, A., Lax, P. D., van Leer, B., On upstream differencing and Godunov-type schemes for hyperbolic conservation laws, *SIAM Review* 25 (1) (1983) 35–61. <https://doi.org/10.1137/1025002>
- [14] Hildebrandt, T., Fottner, L., A numerical study of the influence of grid refinement and turbulence modelling on the flow field inside a highly loaded turbine cascade, *Proceedings of ASME 1998 International Gas Turbine and Aeroengine Congress and Exhibition*, Stockholm, 1998, pp. 1–10. <https://doi.org/10.1115/98-GT-240>
- [15] Hirsch, C., *Numerical computation of internal and external flows: The fundamentals of computational fluid dynamics*, Elsevier, 2007. <https://doi.org/10.1016/B978-0-7506-6594-0.X5037-1>
- [16] Hodis, S., Uthamaraj, S., Smith, A. L., Dennis, K. D., Kallmes, D. F., Dragomir-Daescu, D., Grid convergence errors in hemodynamic solution of patient-specific cerebral aneurysms, *Journal of Biomechanics* 45 (16) (2012) 2907–2913. <https://doi.org/10.1016/j.jbiomech.2012.07.030>
- [17] Holman, J., Fürst, J., Rotated-hybrid Riemann solver for all-speed flows, *Journal of Computational and Applied Mathematics* 427 (2023) 1–13. <https://doi.org/10.1016/j.cam.2023.115129>
- [18] Hwang, C. J., Liu, J. L., Inviscid and viscous solutions for airfoil/cascade flows using a locally implicit algorithm on adaptive meshes, *Proceedings of ASME 1990 International Gas Turbine and Aeroengine Congress and Exposition*, Brussels, 1991, pp. 1–8. <https://doi.org/10.1115/90-GT-262>
- [19] Kiss, T., Schetz, J. A., Moses, H. L., Experimental and numerical study of transonic turbine cascade flow, *AIAA Journal* 34 (1) (1996) 104–109. <https://doi.org/10.2514/3.13028>
- [20] Li, J., Li, X., Ji, L., Yi, W., Zhou, L., Use of blended blade and end wall method in compressor cascades: Definition and mechanism comparisons, *Aerospace Science and Technology* 92 (2019) 738–749. <https://doi.org/10.1016/j.ast.2019.06.045>
- [21] Li, X., Chu, W., Wu, Y., Zhang, H., Spence, S., Effective end wall profiling rules for a highly loaded compressor cascade, *Proceedings of the Institution of Mechanical Engineers, Part A: Journal of Power and Energy* 230 (6) (2016) 535–553. <https://doi.org/10.1177/0957650916649084>
- [22] Longest, P. W., Vinchurkar, S., Effects of mesh style and grid convergence on particle deposition in bifurcating airway models with comparisons to experimental data, *Medical Engineering & Physics* 29 (3) (2007) 350–366. <https://doi.org/10.1016/j.medengphy.2006.05.012>
- [23] Nandan Kumar, K., Govardhan, M., On topology of flow in a turbine cascade, *Journal of Fluids Engineering* 136 (8) (2014) 1–8. <https://doi.org/10.1115/1.4026056>
- [24] Oliveira, R., Justi, G., Lopes, G., Grid convergence study of a cyclone separator using different mesh structures, *Chemical Industry and Chemical Engineering Quarterly* 23 (3) (2017) 311–320. <https://doi.org/10.2298/CICEQ160516044O>
- [25] Roache, P. J., *Verification and validation in computational science and engineering*, Albuquerque, Hermosa Publishing, 1998.
- [26] Salas, M. D., Some observations on grid convergence, *Computers & Fluids* 35 (7) (2006) 688–692. <https://doi.org/10.1016/j.compfluid.2006.01.003>
- [27] Schneider, T., Kožulović, D., Flow characteristics of axial compressor tandem cascades at large off-design incidence angles, *Proceedings of ASME Turbo Expo 2013: Turbine Technical Conference and Exposition*, San Antonio, 2013, pp. 1–13. <https://doi.org/10.1115/GT2013-94708>
- [28] Shin, S., Ragab, S., RANS computation of tip clearance flow in a compressor cascade using an unstructured grid, *Proceedings of the 15th AIAA Computational Fluid Dynamics Conference*, Anaheim, 2001, pp. 1–12. <https://doi.org/10.2514/6.2001-2999>
- [29] Toro, E. F., Spruce, M., Speares, W., Restoration of the contact surface in the HLL-Riemann solver, *Shock Waves* 4 (1) (1994) 25–34. <https://doi.org/10.1007/BF01414629>
- [30] Vassberg, J. C., Jameson, A., In pursuit of grid convergence for two-dimensional Euler solutions, *Journal of Aircraft* 47 (4) (2010) 1152–1166. <https://doi.org/10.2514/1.46737>

- [31] Venkatakrisnan, V., On the accuracy of limiters and convergence to steady state solutions, Proceedings of the 31st Aerospace Sciences Meeting, Reno, 1993, pp. 1–11. <https://doi.org/10.2514/6.1993-880>
- [32] Verwer, J. G., A class of stabilized three-step Runge-Kutta methods for the numerical integration of parabolic equations, *Journal of Computational and Applied Mathematics* 3 (3) (1977) 155–166. [https://doi.org/10.1016/S0377-0427\(77\)80002-2](https://doi.org/10.1016/S0377-0427(77)80002-2)
- [33] Warren, G. P., Anderson, W. K., Thomas, J. L., Krist, S. L., Grid convergence for adaptive methods, Proceedings of the 10th Computational Fluid Dynamics Conference, Honolulu, 1991, pp. 1–13. <https://doi.org/10.2514/6.1991-1592>
- [34] Wilcox, D. C., *Turbulence modeling for CFD*, La Cañada, DCW Industries, 1998.
- [35] Yin, Z., Durbin, P. A., Detached eddy simulation of transition in turbomachinery: Linear compressor cascade, *Journal of Turbomachinery* 144 (3) (2022) 1–9. <https://doi.org/10.1115/1.4052309>
- [36] Zlatev, Z., Dimov, I., Faragó, I., Havasi, Á., Richardson extrapolation: Practical aspects and applications, Berlin, De Gruyter, 2017. <https://doi.org/10.1515/9783110533002>